A Comparison of the Contact Ionization of Cesium on Tungsten with That of Molybdenum, Tantalum, and Rhenium Surfaces

O. K. Husmann*
Hughes Research Laboratories, Malibu, Calif.

Evaluation of the surface ionization of cesium on four porous refractory materials regarding ionization efficiency and critical temperatures is reported. Results from the porous materials are compared with solid surface data. The ionization efficiency of the porous material depends upon the flow rate per pore and, therefore, is directly related to the number of pores per unit area. An optimized emitter has more than 3.10^6 pores/cm². In this case the neutral flux at 10 ma/cm² does not exceed 2.6% under clean surface conditions. The ion engine power efficiency depends upon the critical temperature and current density. Comparison of porous tungsten, rhenium, molybdenum, and tantalum indicates the superiority of tungsten. Power efficiencies for clean and oxygenated porous tungsten at 10 ma/cm² reach between 80 and 90%. At higher current densities the critical temperature is of less importance, and porous rhenium with its higher ionization efficiency becomes more interesting.

Nomenclature

ψ = ion atom resonance charge exchange cross section, cm²
F = neutral flux through the acceleration electrode aperture, per sec
L = ion beam-atom beam interaction length, cm
i = ion current in ions per sec
v = ion velocity, cm/sec
β = ionization efficiency
α = transmission coefficient
V = acceleration potential, volts
p_i = ion perveance, amp/$V^{3/2}$
e = 1.6×10^{-19} C
A = effective emitter surface area, cm²
T_E = emitter temperature, °K
M = atomic mass number
p = alkali vapor pressure, Torr
T_F = alkali temperature, °K
I_{ND} = neutral detector current, amp
q = collimator cross section, cm²
d = distance neutral detector anode to emitter, cm

Introduction

RECENTLY we have been concerned mainly with the comparative evaluation of rhenium, molybdenum, and tantalum with tungsten.[1] It seems to be essential that the melting point by far exceeds the operating temperature of the porous refractory material in order to avoid change of the transmission coefficient during the period of operation. For this reason, platinum and columbium are of less interest and are not included here.

Quite opposite viewpoints are indicated by some theoretical and experimental approaches to the effect of the pore size on the surface ionization on porous material.[2] Therefore, a number of porous tungsten pellets with average pore radii of between 1 and 5 μ have been investigated, each pellet counted and spectral-analyzed.

Oxygen and hydrogen have been introduced into the ultra high vacuum system to control the carbon content in the pellet and to change the surface work function. The electron emission from a porous tungsten emitter at constant cesium flow is compared with the electron emission from solid tungsten in the presence of cesium vapor.

Presented at the AIAA Electric Propulsion Conference, Colorado Springs, Colo., March 11–13, 1963; revision received September 3, 1963. This work was supported by Contract NAS 5-517. The author gratefully acknowledges the assistance of D. Jamba, J. Becker, and J. Mulane in part of this work.

* Senior Member, Technical Staff. Member AIAA.

Pellets under Investigation

The statistical data and transmission coefficients of the experimentally evaluated pellets are combined in Table 1. The X and U pellets are porous tungsten from different manufacturers. In addition to the Re-II rhenium pellet,[1] Re-IV was tested, under clean surface conditions. Counting in general was done after the pellets were polished and the silver or copper filler material removed. The surfaces of the molybdenum and tantalum pellets were etched during polishing and the filler metal was not removed.

All these pellets with the exception of Re-IV were checked by spectral analysis with an Allied Research Laboratories' 2m focal length grating instrument with high purity graphite electrodes. Table 2 presents these analyses. The data for Re-IV are from powder analysis (by a different instrument). All data provided by Table 2 are semiquantitative with the results shown in weight percent. A number of elements, including carbon, are not indicated.

Regarding residual gases, it may be mentioned that the vacuum system is completely free of hydrocarbons with the exception of occasional traces of CH_4. During the bakeout period, the tube is evacuated by an Hg-diffusion pump, and a zeolithe trap prevents backstreaming of hydrocarbons from the mechanical pump.

Prior to surface ionization experiments, the pellets were heated to above 1600°K which proved to be an effective cleaning method. Carbon (carbides), however, with its low vapor pressure can only be removed by the introduction of H_2O or O_2 into the vacuum system.[3] Here O_2 was generated from a BaO_2 source with a partial pressure of between 2.5 and 5×10^{-5} Torr. The pellet temperature was maintained at 1600°K, and CO as well as CO_2 were monitored by a CEC 21-612 mass-spectrometer.[4] Particularly with the U-tungsten pellets, the development of CO_2 and CO is typical after the introduction of O_2 into the vacuum system. (Besides the large amount of oxygen, traces of H_2O, OH, and H_2 are also present during the introduction of O_2.) Introduction of O_2 is started after reaching the lower 8th to 9th scale.

The pellet temperatures are controlled by pyrometer and their spectral emissivities are measured by comparison with black body radiation.[1] Measurements indicate that in the temperature range of interest, between 1100° and 1400°K for all materials under investigation, the spectral emissivity

Table 1 Pellets under investigation

	Weighted density, %	Counted density, %	Mean pore diam, μ	Mean pore distance, μ	Number of pores, cm^{-2}	Transmission coefficient
X-VII	74	77.5	4.0	14.1	3×10^5	1.0×10^{-3}
X-VIII-1 & 2	86.7	84.6	4.3	23.6	1.28×10^5	3.3×10^{-5}
Re-II	82.8	82.4	1.5	6 7	1.49×10^6	1.6×10^{-4}
Re-IV	77	76.3	3.0	9.6	6.25×10^5	$1\ 92 \times 10^{-4}$
Mo-I	76	79.8	1.4	5.6	2×10^6	3.2×10^{-5}
Ta-I	73.6	75	3.6	4.1	1.69×10^6	2×10^{-4}
U-I	70	61.5	1.1	1.8	2.7×10^7	9.1×10^{-5}
U-V	74.6	73.1	1.9	5.2	1.98×10^6	1.7×10^{-4}
U-8-s	75.9	77.7	4.8	16.9	2.1×10^5	7.3×10^{-4}
U-18	72.7	73.4	10.6	29.3	6.3×10^4	1.8×10^{-3}

is not very dependent upon temperature. The spectral emissivities for rhenium, molybdenum, and tantalum, respectively, are 0.47, 0.5, and 0.5 at 1150°C whereas the measured spectral emissivities on porous tungsten range between 0.55 and 0.69 at the same temperature.[1]

It is difficult to obtain consistent data for the total emissivity of porous tungsten; surface effects, in particular carburization, play a major role. Data so far available range between about 0.25 and 0.55 at 1400°K (Gallagher[5]).

Neutral Detector Characteristics

For a better understanding of the neutral detector readings, its essential characteristics are outlined here.

The neutral detector is placed opposite the ion emitting surface and its collimator ($\frac{1}{4}$ in. in diameter and 2 in. long) is well aligned. The outer negative electrode is LN_2 cooled to avoid recirculation of cesium inside the neutral detector. The inner electrode temperature does not exceed 1000°K which is more than sufficient for current densities of 1 μamp and less. The perveance of the detector is 2×10^{-8} for cesium ions, and the potential between cathode and anode never exceeds 30 v, thus avoiding secondary electron emission. Photoeffect at the operating temperature is negligible.[9] A shutter in front of the detector allows the elimination of background readings, and no ions are accelerated toward the detector. The ion beam is electrostatically deflected 90°. Atoms coming from structures that are opposite the detector surface may increase the detector reading. This area can be measured as follows: the intensity of a beam passing an aperture under the angle ϕ to its normal decreases with $\cos^4\phi$. Depending on the collimator length and diameter, its shadowing effect further decreases the "preumbra" area. The outer diameter of the preumbra is the intersection of the collimator diagonal with the structure, and its inner diameter is the extension of the inner collimator wall. As a good approximation, it may be assumed that the atom evaporation density from a structure surface element parallel to the detector surface decreases linearly with increase of the preumbra radius. Assuming cesium saturation conditions on the structure and known structure temperature, its contribution to the detector reading can be computed. In the case of a water cooled structure, the cesium saturation vapor pressure is 5×10^{-7} Torr and the cesium evaporation to the neutral detector is negligible, even when the neutral cesium efflux from the emitter is only 1% of its total efflux. The relatively large cesium ion atom charge exchange cross section with 2.25×10^{-14} cm^2 at 5 kv[6] may be a second possible source of error in the neutral detector reading. Collision ratio at a total flux corresponding to 10 ma/cm^2 and 50% ionization efficiency becomes 6×10^{-3}%, whereas the collision probability decreases with $v^{-0.4}$. At 0% and 100% ionization efficiency, β, there is no interaction between ions and atoms. The interaction reaches its maximum at $\beta = 0.5$. The number of ion-atom resonance charge exchange collisions n is

$$n = \psi FLi/v \tag{1}$$

Measurement of the space charge limited current and the neutral flux $(1 - \beta)$ vs the acceleration potential gives a direct indication of the collisions between atoms and ions in the beam.

$$\frac{d\beta}{dV} = \frac{(\frac{3}{2})p_i V^{1/2}(TM)^{1/2}}{e\alpha pA3.5 \times 10^{22}} \tag{2}$$

and

$$\frac{dI_{ND}}{dV} = -\frac{3qp_i V^{1/2}}{2\pi d^2} \tag{3}$$

In Eq. (2), 100% ionization efficiency in the saturation range is assumed. The actual neutral flux $(1 - \beta^*)$ in this range, therefore, must be added to yield the total neutral flux $(1 - \beta^{**})$ in the space charge limited range.

$$(1 - \beta^{**}) = (1 - \beta^*) + (1 - \beta) \tag{4}$$

Measurements of dI_{ND}/dV revealed excellent agreement with the theoretical curve. Therefore, the interaction between cesium atoms and ions in these experiments is negligible and in agreement with the forementioned evaluation of the resonance charge exchange. Since the cesium vapor pressure is very sensitive to changes in the fuel container

Table 2 Pellet analysis

	Re-II Re	Mo-I Mo	Ta-I Ta	U-I W	U-V W	U-8-s W	U-18 W	Re-IV Re
Be	0.08							
Cu	0.005	0.0003	0.0007					$<10^{-4}$
Fe	0.1	0.2	0.03	0.07	0.02		0.02	10^{-3}
Si	0.04	0.08						$<10^{-4}$
Ni	0.3	0.09	0.009					
Cr	0.2							
Cb			0.3					
Mo		Bal.	0.004	0.03		0.9	0.03	
Ca				0.01	0.003	0.006	0.008	$<10^{-4}$
Al	0.02			0.07	0.06	0.09	0.1	$<10^{-4}$
Ti	0.2							
Mg	0.004							$<10^{-4}$

temperature, small changes in the cesium vapor pressure may affect the accuracy of the above readings.

$$\frac{dI_{ND}}{dT_F} = I_{ND}\left(\frac{1}{T_F}\right)\left(\frac{9290}{T_F} - 1.4\right) \qquad (5)$$

At 10 ma/cm² cesium ion current density and 90% ionization efficiency, a change in the cesium reservoir temperature by 1.0°C results in a 2.3% change of the neutral detector current I_{ND}.

Dependence of the neutral detector current on the emitter temperature is proportional to $-(\frac{1}{2})T_E^{-3/2}$. Small changes in the emitter temperature, therefore, do not affect the readings.

Evaluation of Ionization Efficiency and Critical Temperature on Porous Material

To find a comparative basis for the evaluation of porous tungsten, rhenium, molybdenum, and tantalum pellets as well as for porous pellets in general with regard to ionization efficiency and critical temperature, a number of tungsten pellets with various pore diameters have been investigated.[7]

The porous material serves two purposes: 1) transport of the alkali to the ionizing surface, and 2) surface ionization. Regarding the flow mechanism, the porous material may be treated as a bundle of capillaries, taking tortuosity into account. The main flow mechanism is molecular flow, with $\lambda > \bar{r}$. (λ is the mean free path and $\bar{r}$ the mean pore radius.)

It has been pointed out[1] that high ionization efficiency of the ion propulsion system is desirable. According to the Saha equation in connection with cesium on high work function solid refractory material, ionization efficiencies exceeding 99% are feasible. Of importance is that the surface work function is not reduced by alkali concentrations.[3] Sufficient low surface coverage density can be maintained by condensation out of the gas phase. Moreover, the surface of porous material then acts like a solid surface with regard to ionization, as measured at low current densities with backfeeding.

Cesium supply at higher flow rates by backfeeding, as used in the ion engine, is in contrast to the statistically equal distribution from the gas phase. Alkali gradients first built up around the pore ends, then reduced the surface work function in this area, and finally increased atom evaporation results. For ionization, the atoms have to migrate to low coverage surface areas. To approach a surface distribution with alkali backfeeding, as from the gas phase, increase in the number of pores per unit area or decrease in the flow rate per pore is the consequence. The pore diameter only indirectly affects the surface ionization. All pellets under investigation are, therefore, compared on the basis of number of pores per cm².

The measured ionization efficiency of a number of different tungsten pellets coincides in the investigated range of current densities when corrected for equal flow per pore. The number of pores per cm² was computed from measured mean pore diameter and pore distance (Table 1). The pellets compared have pore radii of between 1 and 5 μ. The neutral flux is plotted vs the ion current density with a constant number of pores per cm² as the parameter in Fig. 1. For comparison, the neutral flux from solid tungsten vs current density is shown. (ϕ_e = 4.7 ev.) As indicated, the neutral flux decreases considerably with increase of pores per cm², and with 3×10^6 pores per cm² the neutral efflux at 10 ma/cm² is less than 3%. In the range for $N \geq 10^6$ conducting pores per cm², the neutral flux in percent is related to the cesium ion current density in amp/cm² and the number of pores per cm² by

$$\log(1 - \beta^*) = \tfrac{1}{2}(\log j + 9.296 - \log N) \qquad (6)$$

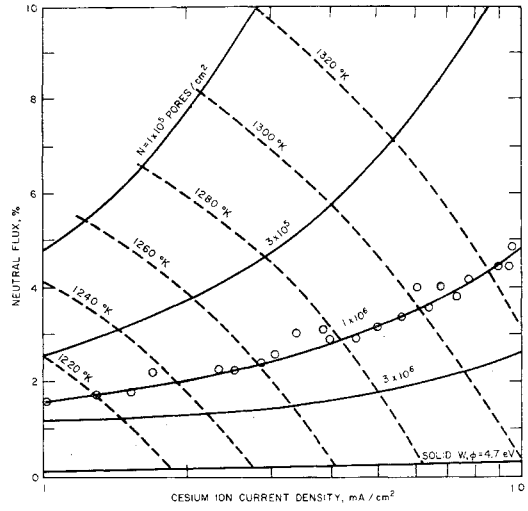

Fig. 1 Dependence of the neutral flux on the cesium ion current density. (Parameter is the number of pores/cm². Dashed lines are critical temperatures.)

By decreasing N, the deviation between (6) and the experimental data increases due to the fact that $(1 - \beta^*)$ increases more steeply than is proportional to $N^{-1/2}$.

So far, only the neutral flux from pellets with pore radii of 2μ or larger and two pellets of 1μ pore radius is consistent. In general, pellets with mean pore radii in the area of 1μ show somewhat lower ionization efficiencies than expected; this may be caused by partial clogging. Re-check of the transmission coefficient of two pellets with $\bar{r} \sim 1\mu$ after longer heat treatment indicated an increase which may correspond to a larger number of open pores. In Fig. 1, some critical temperature isothermes are given over a range from solid tungsten[9] to 1×10^5 pores per cm², in addition to the neutral flux.

In Fig. 2, the number of pores per cm² is plotted vs the current density, with the neutral efflux as parameter with ionization efficiencies between 98.5 and 95%. An empirical equation can be deducted from these curves connecting pore spacing, pore diameter, current density, and neutral flux:

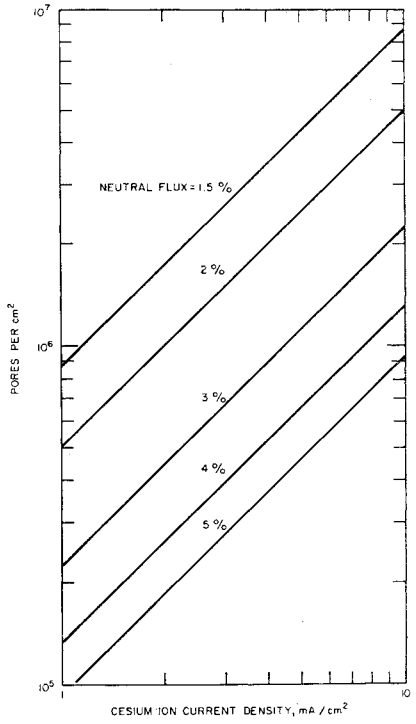

Fig. 2 The number of pores/cm². N is proportional to ion current density at constant neutral efflux.

$$d = 10^4(j \times N_0)^{-1/2} - 2\bar{r} \quad (7)$$

with

d = pore spacing, μ
j = ion current density, ma/cm^2
$\bar{r}$ = mean pore radius, μ

and with N_0 depending upon the required neutral flux. These data are given in Table 3.

The neutral flux from porous tungsten, rhenium, molybdenum, and tantalum pellets is plotted in Fig. 3 vs the cesium ion current density considering an equal number of pores per cm^2 (1×10^6). The four refractory materials show the steep changeover from low to high ionization efficiency. It was possible to operate tungsten and rhenium under clean surface conditions with electron work functions of 4.7 ev and 4.9 ev (see Refs. 10 and 11). The neutral flux from rhenium is somewhat lower than that from tungsten. The neutral flux from porous molybdenum exceeds that expected in connection with 4.24 ev work function.[12] The measured electron work function is 3.8 ev, in good agreement with that published for Mo_2C.[14] The electron work function, measured on porous tantalum is 4.1 ev, close to published data for clean solid tantalum (4.19 ev).[13] This explains the higher measured ionization efficiency on tantalum vs that of Mo. At 1 ma/cm^2 the neutral flux from tantalum corresponds to a work function of 4.3 ev. Carburized (refractory) metal surfaces have a different work function compared with that of the clean material. Carburized tungsten has been investigated repeatedly and it has been recently reported that $\Phi = 4.58$ ev ($A = 190$ amp cm^{-2} deg^{-2}) vs $\Phi = 3.6$ ev from another publication.[14]

As described earlier, rhenium and tungsten were checked by mass-spectrometer for presence of their carbides. O_2 was introduced into the vacuum system from a BaO_2 source at a partial pressure close to 5×10^{-5} Torr. During the introduction of O_2, the pellet temperature was maintained close to 1600°K and the development of CO_2 and CO was monitored.[3, 4]

Carbon has been at least partially removed from Ta-I and Mo-I by the introduction of air into the vacuum system through an artificial leak.

Three existing theoretical approaches attempt to correlate the neutral efflux with the pellet structure and the pellet temperature. One of these theories agrees relatively well with our data taking into consideration the total ion current and 0.2 fraction of the total cross section open to flow in combination with 1 μ pore radius.[2] The pore radius and the open fraction of the surface yield the number of pores per cm^2 for comparison. It may be mentioned that published basic data for quantitative evaluation of such an approach spread widely. Instead of employing a pore radius it is considered more favorable to define a radius at which the alkali surface concentration rapidly changes to a low value. Because of the instability of a medium covered surface in the case of ion extraction such a boundary must exist. To keep this radius for ion emission relatively constant at increasing flow rates, the initial surface temperature must also be increased.

These critical temperatures are added in Fig. 1 and cover a range of ion current densities from 1 to 10 ma/cm^2 and up to 10^5 pores per cm^2. The critical temperatures for the solid tungsten curve are from Taylor and Langmuir.[9] With a

Table 3 Constants to Eq. (7)

$(1 - \beta^*)\%$	N_0(cm^{-2})
1.5	8.5×10^5
2.0	5.0×10^5
3.0	2.2×10^5
4.0	1.3×10^5
5.0	9.4×10^4

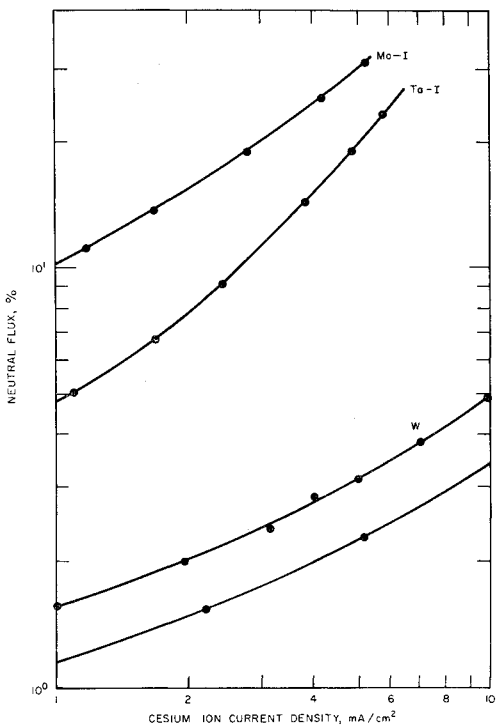

Fig. 3 Measured neutral flux from rhenium, tungsten, tantalum, and molybdenum compared on the basis of 10^6 pores/cm^2.

decreasing number of pores per cm^2, the critical temperature increases first slowly, then more rapidly. Figure 4 plots the relationship between critical temperature and number of pores per cm^2. At 10 ma/cm^2 and 10^6 pores per cm^2 the critical temperature exceeds that of solid tungsten by 31°K, and with 10^5 pores per cm^2 by 123°K. For fuel and power economy as well as for an increase in the lifetime of the ion engine, it is therefore necessary to develop a porous material with a maximum of pores per unit area. On the other hand, clogging forms the limit toward very fine pores. Minimum pore spacing due to free surface area for ion migration is under investigation. 3×10^6 pores per cm^2 seems to be a reasonable compromise from Figs. 1 and 4. At this pore number and 10 ma/cm^2 ion current density, the critical temperature exceeds that for solid tungsten by approximately 17°K, and the ionization efficiency reaches more than 97%. The points in Fig. 4 at 10^8 pores per cm^2 are for solid tungsten.

Figure 5 shows the critical temperatures for rhenium, tungsten, molybdenum, and tantalum which are compared with those for porous tungsten and molybdenum published by Lebedev, et al.[15] (No corrections for equal pore number per cm^2 are made.) Our critical temperature on molybde-

Table 4 Critical temperature equation constants

	A	B	Number of pores, cm^{-2}	Literature
Solid tungsten	14×10^3	8.764		9
Solid tungsten	12.6×10^3	6.8		16
[a] Oxygenated porous tungsten	19.5×10^3	11.12		
Porous tungsten	15.38×10^3	9.28		15
[a] Porous tungsten	12.5×10^3	7.37	1×10^6	
Solid rhenium	17.7×10^3	9.4		16
[a] Porous rhenium	13.08×10^3	7.06		
Solid molybdenum	12.4×10^3	6.9		16
Porous molybdenum	13.84×10^3	8.33		15
[a] Porous molybdenum	13.0×10^3	7.48	2×10^6	
Solid tantalum	12.9×10^3	6.9		16
[a] Porous tantalum	12.81×10^3	6.56	1.69×10^6	

[a] Measured by author.

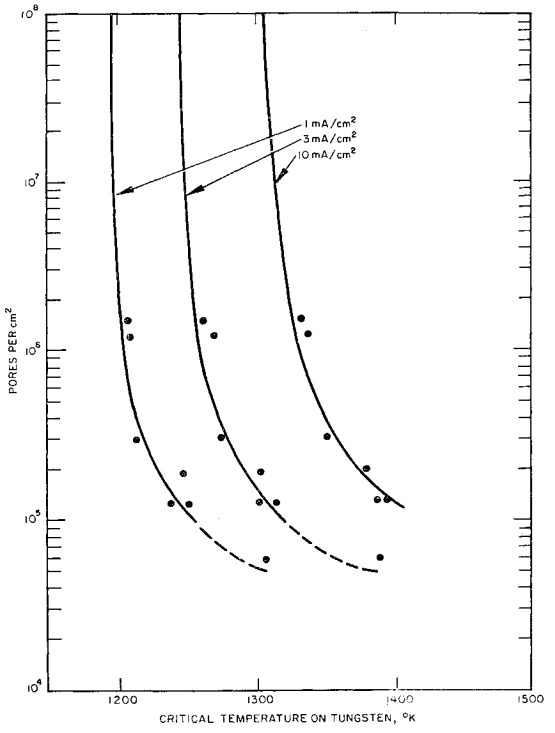

Fig. 4 Dependence of the critical temperature on the pore number/cm².

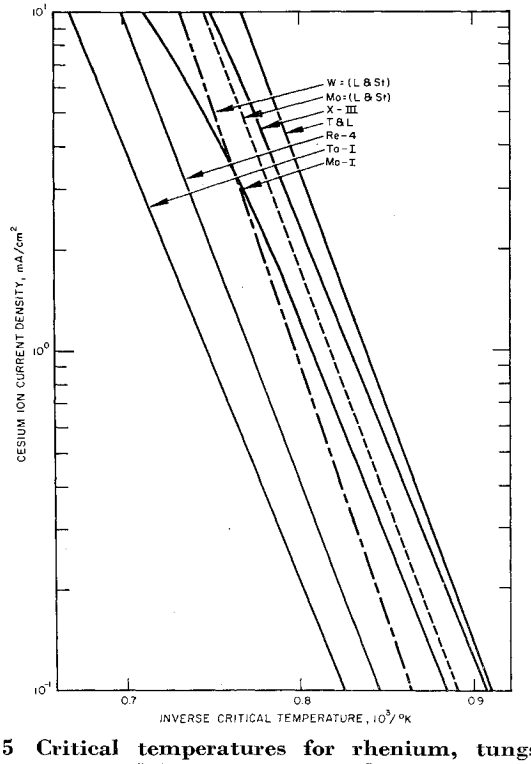

Fig. 5 Critical temperatures for rhenium, tungsten, molybdenum and tantalum.

num somewhat exceeds that of Lebedev; on the other hand, our porous tungsten data are lower. Direct comparison between Lebedev's and these data is not possible because of the lack of statistical information. Of the four refractory materials investigated, Ta has the highest critical temperature followed by rhenium.†

† The critical temperatures of porous tungsten and molybdenum are close. Mo-I has 1.66 times as many pores as X-III. A direct comparison between them is limited because of the measured low work function of Mo-I (3.8 ev).

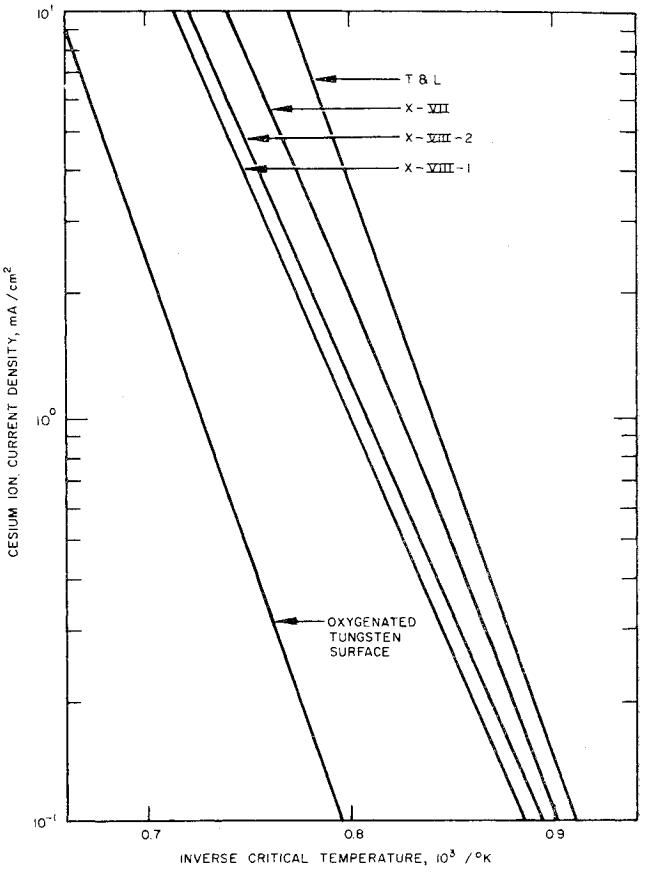

Fig. 6 For check of the accuracy of our readings, two pellets of the type X-VIII have been tested. The dT_C at 10 ma/cm² does not exceed 16°K, and $dT_C/T_C \simeq 1\%$.

Some critical temperatures for tungsten pellets with clean surfaces, but different numbers of pores per cm² (Table 1) are plotted in Fig. 6. Of the X-VIII-type tungsten material, two different pellets have been investigated for comparison, and as indicated, the measured critical temperatures are within 16°K. Agreement of their ionization efficiency is within 1%. In the range from 0.1 ma/cm² to 10 ma/cm², the critical temperatures for cesium on tungsten, rhenium, molybdenum, and tantalum follow an equation in the form

$$T_C = A/B - \log j; \ ^\circ\mathrm{K} \tag{8}$$

A and B are constants; j = ion current density, amp/cm². The critical temperature of oxygenated porous tungsten exceeds that of all the investigated materials. By comparison of the critical temperature and ionization efficiency of molybdenum with that of tungsten, the latter is of advantage. In spite of its relatively high critical temperature, rhenium is the most suitable material if a minimal neutral efflux is required.

With regard to the beam power and the radiated energy (from the emitter) the power efficiency of the ion engine increases strongly with the ion current density. If the ion beam power is related to the ion gun perveance p_i it follows for engine efficiency with accel/decel ratio 2/1

$$\eta = \frac{1}{1 + (3\epsilon\sigma T^4/\frac{1}{2}j^{5/3}p_i^{-2/3})} \tag{9}$$

η = power efficiency
j = current density, amp/cm²
p_i = the ion perveance, 2.5×10^{-9} $(A \times V^{-3/2})$
ϵ = the total emissivity
σ = 5.67×10^{-12} (W cm^{-2} deg^{-4})

Here the total emissivity is 0.3 (see Ref. 5) and the heater efficiency κ is 33%; this means that one-third of the heater

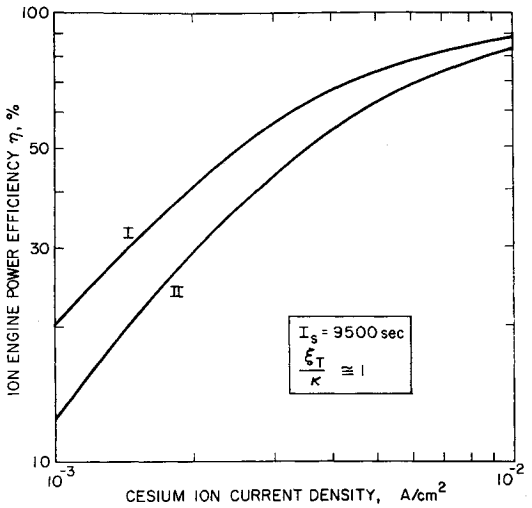

Fig. 7 Power efficiency for clean and oxygenated porous tungsten.

input power is radiated from the emitter surface area. The lower curve, Fig. 7, corresponds to oxygenated tungsten and the upper one to clean porous tungsten. For clean tungsten at 1 ma/cm² cesium ion current density, the power efficiency does not exceed 20%, but at 10 ma/cm² it reaches 88%. The advantage of a clean emitter surface is obvious.

It is possible to make an approach to the critical surface temperature if data on electron emission in presence of cesium vapor are available by combination of the Saha and the Richardson equation.[16] Extrapolation of these data to alkali surface ionization on porous material with backfeeding is limited by the fact that electron emission from porous material in the presence of alkali vapor is different from that of the solid material and that the surface ionization on a patchy surface takes place on the higher work function patches.[17] In contrast, the electron emission originates from the low work function areas. In Fig. 8, both upper curves I and II give the electron emission from porous tungsten, (made here from spherical tungsten powder). The measured electron work function of the clean surface is 4.63 ev (A = 110 amp/cm² deg²) (curve III). With the porous material, two cesium arrival rates have been used at the surface: 1) 8.6×10^{16} atoms/sec cm², and 2) 1.1×10^{18} atoms/sec cm². For comparison, electron emission from solid tungsten with 10^{16} atoms/sec cm² is plotted.[9] The change in electron

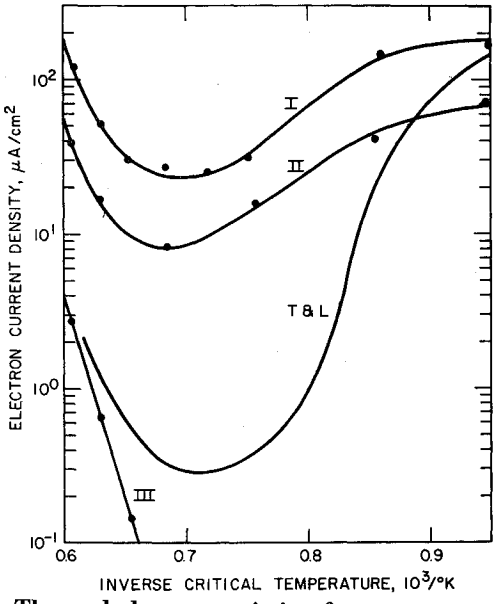

Fig. 8 Thermal electron emission from porous tungsten in presence of cesium.

emission due to cesium coverage from the solid surface exceeds that from the porous surface.

Surface Contaminants

Surface contaminants such as an adsorbed monolayer or partial monolayer of any gas change the surface work function. In general, a vacuum system contains a relatively large amount of H_2 and N_2, mostly from outgassing metal parts. Hydrogen increases the surface work function of W_{113} by 0.43 ev.[18] It is desorbed below the operating temperature of the emitter. The same happens to nitrogen.[19] If adsorbed on W_{113}, the surface work function increases by 0.35 ev; in the case of CO adsorption on the same tungsten surface (113), the work function rises by 0.86 ev.[20] According to Trapnell[21] these gases are chemisorbed on W, Mo, and Ta. (This is also probably true on Re.) The amount of adsorption is temperature dependent and, in the temperature range of interest, relatively low, although oxygen, with its high desorption energy, is an exception.[22] Condensation out of the gas phase is proportional to the condensation probability χ and decreases with increasing surface coverage:

$$\chi = \gamma f(\theta) \exp[-E/kT] \qquad (10)$$

with γ the condensation coefficient, θ the surface coverage with regard to a monolayer, and E the adsorption activation energy. According to Becker, et al.,[3,23] at low coverage the oxygen condensation probability on tungsten is 0.14; this figure decreases to 0.04 after less than half of the surface is covered. Adsorption of oxygen takes place rapidly with 6×10^{-8} Torr partial pressure on tungsten at 300°K. After

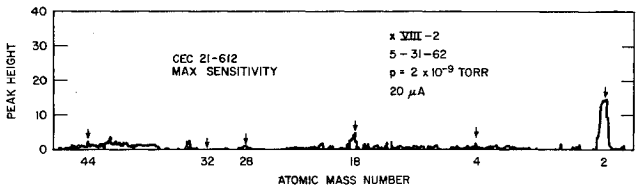

Fig. 9 Residual gas spectrum at 2×10^{-9} Torr.

$2\frac{1}{2}$ min the surface work function has increased by 0.3 ev.[23] To maintain clean surface conditions for some time, the partial pressure of oxygen must be on the 10th scale or below. An adsorbed oxygen monolayer would increase Φ by 1.6 ev.[22, 24]

The partial pressures in the lower mass range are controlled with a CEC 21-612 mass spectrometer. Figure 9 shows a typical mass spectrogram at a total pressure of 2×10^{-9} Torr; the electron current is 20 μamp and the main peak is H_2. The sensitivity of the mass spectrometer for hydrogen is considerably lower than that for nitrogen and hydrocarbons. This reading was taken approximately 24 hr after pumping down with both heaters inside the tube at operating temperature. At the maximum electron emission of 100 μamp with the 180 liter/sec ion pump running, the partial pressure of oxygen is beyond the range of the mass spectrometer. If there are traces of free oxygen, they should accumulate with the pump cut-off over a period of time; however, cut-off times of 2 hr and more resulted only in small increase of the mass 28 and mass 2 peaks. (Factor 1.45 for M-28.) No oxygen was detected. It was during this experiment that the cesium capsule was broken. When the heater was shut off for several hours and then flashed at about 1800°K, gas evolution was analyzed as hydrogen and nitrogen. From these results and control of the surface work function without flashing the filament over several days it is concluded that the oxygen partial pressure is below 10^{-10} Torr. (It is interesting to note that after shut-off the ion pump still pumps some gases onto its clean Ti surfaces.) These results confirm our earlier control of the oxygen content by surface work function measurements.[1]

Some time ago we reported hysteresis of cesium and potassium with surface ionization on porous tungsten, and the same was observed with cesium on the other refractory materials under investigation. Zanderberg[25] observed this effect in the pre-threshold region with potassium on solid tungsten and tries to explain it as an interaction of the alkali molecules on the emitter surface. At the beginning of the ion current experiments this effect was strong and decreased relatively rapidly to a few degrees. Figure 10 shows this effect on rhenium after the introduction of oxygen into the vacuum system. In comparison with oxygen, the partial pressures of the other residual gases are negligible. This experiment implies that oxygen is one contaminant causing hysteresis in the threshold region of surface ionization on refractory materials. Introduction of hydrogen into the system at pressures in the range of 10^{-5} Torr did not change the surface conditions. The flow rate of cesium also was not affected by either hydrogen or oxygen in this pressure range with flow rates of 8.1×10^{11} and 2.8×10^{11} atoms/sec, respectively. Both gases were introduced on the critical surface side, not on the fuel side.

Correlation between the Transmission Coefficient and the Structure of the Porous Material

Correlation between the number of pores per cm², the neutral flux, and the critical temperature was discussed in the preceding section. With regard to the flow mechanism, of interest is the connection between the transmission coefficient and the statistical information from these pellets. The molecular flow per pore (with $L \gg \bar{r}$) is proportional to

$$(\tfrac{8}{3})(\bar{r}^3/L)\pi \qquad (11)$$

Regarding the alkali flow, the porous material may behave like a bundle of capillaries because then the total flow must be proportional to (11) multiplied by the total number of pores.

$$\alpha = \frac{8\pi\bar{r}^3NA}{3L\xi} \qquad (12)$$

where α is the transmission coefficient (ratio of passing through to impinging atoms), $\bar{r}$ is the mean pore radius, L is the pellet thickness, N is the number of pores per cm², A is the pellet surface area, and ξ may be interpreted as tortuosity. Because all pore cross sections appear in a single

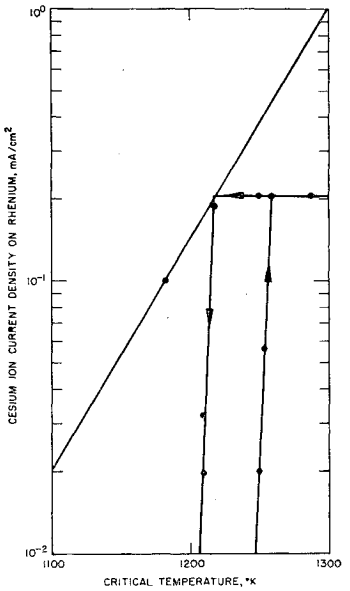

Fig. 10 Hysteresis at the threshold for surface ionization on porous rhenium.

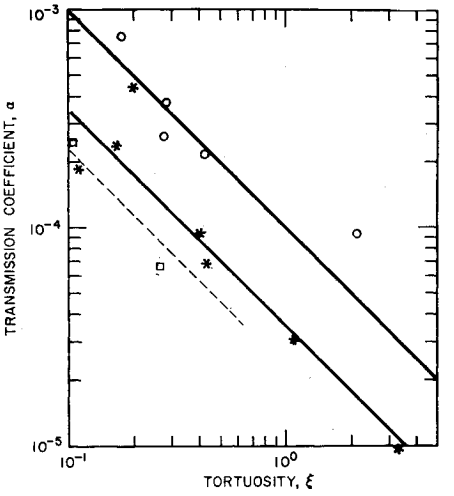

Fig. 11 Tortuosity of porous materials related to the transmission coefficient.

capillary of the porous material, $\bar{r}$ was weighted with its relative frequencies in the first power. None of the pellets statistically investigated so far showed Gauss distribution of the pore radii. This may result from the nongaussian distribution in the original powder and also may be partly dependent upon the low resolution of the counting technique in the submicron range.

The transmission coefficient α is plotted vs the tortuosity ξ in Fig. 11. From Eq. (12) one would anticipate a straight line on double log paper. The X and Y pellets[1] (including Re-II and Mo-I) follow the theoretical slope relatively closely whereas the U pellets fitting the upper slope have a wider range of dispersion. It is known that the pellets fitting the upper slope have been sintered at lower temperatures than have those following the lower slope. The factor which appears here as the parameter may be identified as consolidation. The materials sintered at higher temperature have a lower transmission coefficient at the same tortuosity.

The data available so far are not sufficient to design optimized porous pellets. To achieve both high ionization and conductance (to reduce the consolidation), narrow distribution of the grain sizes seems to be essential. Separation is easiest with spherical tungsten powder, which, if treated properly, also offers the advantage of dense packaging[26] and low consolidation.

Life Test

Five different pellets were under continuous test for 11 months. The conditions were: pellet temperature close to 1440°K and passage of small amounts of cesium through the pellets. The test was done under ultra high vacuum. H_2O, OH, and some mass 28 were the main residual gases. Prior to being incorporated into the life test, all pellets were flow-rate checked several times, and their ionization efficiency and critical temperature measured. Some results of this experiment after 10 months duration are indicated in Fig. 12. Pellets incorporated are X-II, X-III, X-V, X-VII, and Y-III.[1] Plotted is the time of test vs the transmission coefficient. Particularly for the X-II and X-III pellets, the transmission coefficient increases during the time of test (average pore diameter, 2μ) whereas the transmission coefficient of X-VII with 4μ mean pore diameter is constant. These data are preliminary because the transmission coefficient depends upon the pellet geometry which will be checked after 12 months of test.

It is interesting to mention that the transmission coefficients have been measured each time at a temperature close to 1600°K after cleanup. These life test results are in con-

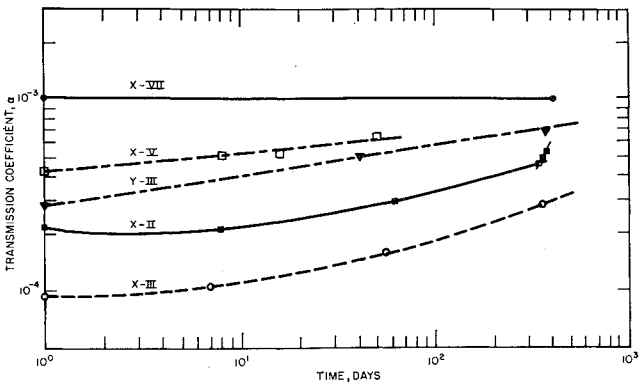

Fig. 12 Variation of the transmission coefficient with the time of operation.

trast to the theory of continuous sintering of the porous material.[27]

Conclusions

With regard to ion engine power efficiency, tungsten, because of its relatively low critical temperature, is the suitable material for surface ionization. Decrease of neutral efflux and critical temperature with increasing number of pores per unit area implies the development of fine grain pellets. Emphasis is given to spherical powders with narrow grain size distributions.

References

[1] Husmann, O. K., "Experimental evaluation of porous materials for surface ionization of cesium and potassium," *AIAA Progress in Astronautics and Aeronautics: Electric Propulsion Development*, edited by E. Stuhlinger (Academic Press Inc., New York, 1963), Vol. 9, pp. 195–217.

[2] Reynolds, T. W. and Kreps, L. W., "Gas flow, emittance and ion current capabilities of porous tungsten," NASA TN D 871 (1961); also Shelton, H., "Surface diffusion studies of cesium on tungsten," IAS-ARS Preprint 61-85-1779 (1961).

[3] Becker, J. A., Becker, E. J., and Brandes, R. G., "Reactions of oxygen with pure tungsten and tungsten containing carbon," J. Appl. Phys. **32**, 411–423 (1961).

[4] Young, J. R., "On the interaction of oxygen with incandescent filaments," presented at 19th Annual Conference on Physical Electronics at Mass. Inst. Tech., Cambridge, Mass. (March 1959).

[5] Gallagher, H. E., private communication (January 1962).

[6] Chen, C. L. and Raether, M., "Collision cross section of slow electrons and ions with cesium atoms," Phys. Rev. **128**, 2679–2682 (1962); also Marino, L. L., Smith, A. C. H., and Caplinger, E., "Charge transfer between positive cesium ions and cesium atoms," Phys. Rev. **128**, 2243–2250 (1962); also Chkusaeli, D. V., Nikoleishvili, U. D., and Guldamashvili, A. I., "Resonance charge exchange of positive alkali metal ions," Bull. Acad. Sci. USSR, Phys. Series **24**, 972–976 (1960); also Estermann, I., Foner, S. N., and Stern, O., "The mean free path of cesium atoms in helium, nitrogen and cesium vapor," Phys. Rev. **71**, 250–257 (1947).

[7] Summary Progress Report, Phase II, "Design, fabrication and testing of a cesium ion rocket engine," Contract NAS 5–517 (September 1, 1961 through August 30, 1962) pp. 95–119.

[8] Becker, J. A., "The life history of adsorbed atoms, ions and molecules," Ann. N. Y. Acad. Sci. **58**, 723–740 (1954).

[9] Taylor, J. B. and Langmuir, I., "The evaporation of atoms, ions and electrons from cesium films on tungsten," Phys. Rev. **44**, 423–458 (1933).

[10] Reimann, A. L., "The surface ionization of potassium on tungsten," Phys. Rev. **45**, 898 (1934); also Smith, G. F., "Thermionic and surface properties of tungsten crystals," Phys. Rev. **94**, 295–308 (1954); also Drechsler, M. and Mueller, E. W., "Zur Feldelektronenemission and Austrittsarbeit einzelner Kristallflaechen," Z. Phys. **134**, 208–221 (1953).

[11] Levi, R. and Espersen, G. A., "Preparation of rhenium emitters and measurement of their thermionic properties," Phys. Rev. **78**, 231–234 (1950); also Anderson, J., Danforth, W. E., and Williams, III, A. J., "Workfunction and thermal desorption in the system thorium on rhenium," J. Appl. Phys. **34**, 2260–2269 (1963).

[12] Gardner, G., Anthony, R. L., and Coomes, E. A., "Thermionic emission from single crystal molybdenum," Bull. Am. Phys. Soc. **6**, 422 (1961); also Herring, C. and Nichols, M. H., "Thermionic emission," Rev. Mod. Phys. **21**, 185–270 (1949).

[13] Fiske, M. D., "The temperature scale, thermionics and thermatomics of tantalum," Phys. Rev. **61**, 513–519 (1942).

[14] Rittner, E. S. and Levi, R., "Role of carburization in the suppression of emission from barium activated tungsten and molybdenum surfaces," J. Appl. Phys. **33**, 2336–2341 (1962); also Baz-Taymas, E., "Elektronen Emissionsmessungen an Systemen Wolfram Kohlenstoff and Molybdaen-Kohlenstoff," Z. Angew. Math. Phys. **2**, 49–51 (1951); also Ingold, J. H., "Thermionic properties of some refractory metal carbides," J. Appl. Phys. **34**, 2033–2039 (1963); also Zubenko, Yu. V. and Sokols'kaya, L. L., Soviet Phys.-Tech. Phys. **7**, 270–272 (1962); also Marchuk, M. P., "Evaporation of barium from surfaces of certain metals," Radio Eng. Electron. **2**, 13–30 (1957); also Ivey, H. F., "Thermionic electron emission from carbon," Phys. Rev. **76**, 567 (1949).

[15] Lebedev, S. Ya., Stavisskii, Yu. Ya., and Shut'ko, Yu. V., "Surface ionization of cesium in diffusion of cesium vapor through porous molybdenum," Soviet Phys.-Tech. Phys. **6**, 836 (1962).

[16] Reynolds, Th. W., "Estimation of critical temperature for surface ion currents from electron emission data," NASA TN D 1307 (1962).

[17] Zemel, J., "Surface ionization phenomena on polycrystalline tungsten," J. Chem. Phys. **28**, 410–413 (1958).

[18] Gomer, R., Wortman, R., and Lundy, R., "Mobility and adsorption of hydrogen on tungsten," J. Chem. Phys. **26**, 1147–1164 (1957); Mueller, E. W., "Feldemission," Ergeb. Exakt. Naturw. **27**, 290–360 (1953); also Eisinger, J., "Properties of hydrogen chemisorbed on tungsten," J. Chem. Phys. **29**, 1154 (1958).

[19] Suhrmann, R., "Elektronische Wechselwirkung bei der Chemiesorption an elektrisch leitenden Oberflaechen," Z. Elektrochem. **60**, 804–815 (1956); also Eisinger, J., "Electrical properties of nitrogen adsorbed on tungsten," J. Chem. Phys. **28**, 165–166 (1958).

[20] Eisinger, J., "Adsorption of CO on tungsten and its effect on the work function," J. Chem. Phys. **27**, 1205–1206 (1957).

[21] Trapnell, B. M. W., *Chemisorption* (Butterworths Scientific Publications Ltd., London, 1955).

[22] Mueller, E. W., "Die Adsorption von Sauerstoff auf Wolfram nach Beobachtungen," Z. Elektrochem. **59**, 372–379 (1955).

[23] Morgulis, N. D. and Naumovets, A. G., "Kinetics of formation and some attributes of oxygen films adsorbed on tungsten," Bull. Acad. Sci. USSR, Phys. Ser. **24**, 657–665 (1960); also Haque, C. A. and Donaldson, E. E., "Continuously oxygenated tungsten as a surface ionization source," Rev. Sci. Instr. **34**, 409–412 (1963); also Dyubua, B. Ch., Pekarev, A. I., Popov, B. N., and Tylkina, M. A., "Thermionic emission of W-Ti and W-Hf alloys and its dependence on oxygen pressure," Radio Eng. Electron. **7**, 1463–1470 (1962).

[24] Gomer, R. and Hulm, J. K., "Adsorption and diffusion of oxygen on tungsten," J. Chem. Phys. **27**, 1363–1376 (1957).

[25] Zandberg, E. Ya., "Surface ionization of potassium atoms and K Cl and Cs Cl molecules on tungsten filaments in electric fields up to 2 MV/cm," Soviet Phys.-Tech. Phys. **27**, 2399–2409 (1957).

[26] Husmann, O. K., "Diffusion of cesium and ionization on porous tungsten," *ARS Progress in Astronautics and Rocketry: Electrostatic Propulsion*, edited by D. Langmuir, E. Stuhlinger, and J. Sellen Jr. (Academic Press, New York, 1961), Vol. 5, pp 505–521.

[27] Anglin, A. E., Jr., "Problems of porous tungsten ionizers for cesium electric propulsion systems," presented at the Natl. Soc. Aerospace Material and Process Engineers Spring Symposium on Space Power Systems Materials, Philadelphia, Pa. (June 3–5, 1963); also Kothari, N. C., "Sintering kinetics in tungsten powder," J. Less Common Metals **5**, 140–150 (1963).